

NATIONAL ADVISORY COMMITTEE FOR AERONAUTICS

TECHNICAL NOTE 2173

DENSITY FIELDS AROUND A SPHERE AT

MACH NUMBERS 1.30 AND 1.62

By Paul B. Gooderum and George P. Wood

Langley Aeronautical Laboratory
Langley Air Force Base, Va.



Washington
August 1950



NATIONAL ADVISORY COMMITTEE FOR AERONAUTICS

TECHNICAL NOTE 2173

DENSITY FIELDS AROUND A SPHERE AT

MACH NUMBERS 1.30 AND 1.62

By Paul B. Gooderum and George P. Wood

SUMMARY

Interferograms were taken of the flow around a sphere at Mach numbers of 1.30 and 1.62. The results of the evaluation of these interferograms are shown as plots of contours of constant density ratio in the flow field around the sphere and as the distribution of flow variables along the axis of symmetry between the shock wave and the sphere. In appendixes the theory of the analysis is reviewed, sources of error are discussed, and the detailed procedure used in the evaluation of the interferograms is described.

INTRODUCTION

One of the flow problems currently receiving attention is that of the flow behind detached shock waves. The present paper gives experimental data on the flow behind the detached shock waves on a sphere. These data consist principally of density distributions around spheres and were obtained for two supersonic Mach numbers by analysis of interferograms. Previous investigations of axially symmetric flow by interferometry can be found in reference 1.

For the convenience of those interested in the application of interferometry to the study of axially symmetric flow fields, the symbols used are given in appendix A and the theory of the analysis is reviewed in appendix B. A discussion is given in appendix C of the sources of error and the accuracy of the results obtainable from interferograms of axially symmetric flow. (This discussion is somewhat similar to those given in references 1 and 2.) Because reasonable accuracy in the results requires that much care be taken in measuring and in plotting fringe shifts, a detailed description of the computational procedure that was used to obtain the final results is given in appendix D. A table of the coefficients for 50 zones for use in the Weyl method of evaluation has been calculated and is also given.

APPARATUS

The test setup consisted principally of a supersonic-jet apparatus that gave a 3-inch-square free jet and an interferometer with 4-inch-square plates. This apparatus has been described in reference 3. The only change in the apparatus was a change in the film magazine to permit the use of 70-millimeter film rather than the 35-millimeter size previously used. Two different Mach numbers were obtained by using two supersonic nozzles similar to those described in reference 3. The test model was a steel sphere $1/2$ inch in diameter that was supported from behind by a sting $1/8$ inch in diameter.

RESULTS AND DISCUSSION

Interferograms

An interferogram that showed the undisturbed fringes in the test section was taken with no flow (fig. 1) and then an interferogram of the flow around the sphere at Mach number 1.30 was taken (fig. 2). The same procedure was followed at a flow Mach number of 1.62; the no-flow interferogram is shown in figure 3 and the flow interferogram, in figure 4. Cross sections were drawn on the flow interferograms perpendicular to the axis of symmetry. The variation of density along each cross section was then obtained by the method described in appendixes B and D. A plot of the ratio of density along the cross section to free-stream density was made for each cross section.

Density Distributions

The plots of density ratio along the cross sections were used for plotting contours of constant density ratio in the flow field around the sphere. Experimental points taken from the unfaired plots of density ratio are shown in figure 5. The curves that are shown are faired through these points.

The method of analysis of the interferograms that was used has the disadvantage that the results obtained are inaccurate in a small region immediately behind a discontinuity in the density. (The reason for the inaccuracy is explained in appendix C.) Because of this inaccuracy in the results immediately behind the shock wave, points on the plots of density ratio that were near the shock wave and that were obviously in error were not included in figure 5. For each contour in figure 5, therefore, a small region adjacent to the shock wave exists in which experimental points have not been obtained. The density contours have

not been extended through this region to the shock wave. On the shock wave, however, the correct location of the intersection of each contour with the shock wave has been indicated. The locations of the intersections were obtained from the equation for the density ratio across a two-dimensional oblique shock wave with use of measured slopes of the shock wave.

The magnitude of any systematic errors in the contours shown in figure 5 is not known. The uncertainty in the location of the contours, aside from any systematic errors, is believed to be not larger than plus or minus approximately one-half the distance between adjacent contours.

Flow Variables along Axis

The distribution of the flow variables along the axis of symmetry is of interest. The region of the axis is, however, a region of relatively large error. In order to obtain what are thought to be the best values of density ratio along the axis, the values at the axis, obtained by fairing the plots of density ratio for each cross section, were used to plot the variation of density ratio along the axis between the shock wave and the sphere (fig. 6). Immediately behind the normal part of the shock wave, the density ratio is well-known from the Rankine-Hugoniot relations. At the nose of the sphere, the correct value of the stagnation density is also known. These theoretical values were used in fairing the curves shown in figure 6 through the experimental points. The density ratios along the axis given by the faired curves have also been converted to ratio of static pressure to stagnation pressure (fig. 7). The distribution of density ratio along the axis has also been converted into the distribution of Mach number shown in figure 8. (The stagnation temperature for the free-stream Mach number of 1.30 was 524.4° F abs. and for Mach number 1.62 was 533.1° F abs. The free-stream density for Mach number 1.30 was 0.003215 slug/cu ft and for Mach number 1.62 was 0.003501 slug/cu ft.)

The variation of density ratio along the surface of the sphere for Mach number 1.62 is shown in figure 9. The experimental points were taken from the plots of density ratio along each cross section.

CONCLUDING REMARKS

Experimental data on the flow around spheres at supersonic speeds have been presented. Although greater accuracy in the data would be desirable, the data given herein are accurate enough that they should

be of use in checking and evaluating theoretical treatments of the problem of predicting the flow behind detached shock waves.

Langley Aeronautical Laboratory
National Advisory Committee for Aeronautics
Langley Air Force Base, Va., June 12, 1950

APPENDIX A

SYMBOLS

a	radius of first zone
$A_{k,i}$	coefficient
d	axial distance from center of curvature of shock wave
i	number of zone at which density is required
k	zone number
L	distance through test section or through disturbance
M	Mach number
N	number of outermost zone
n	index of refraction
p	pressure
r	radial distance from axis of symmetry
R	radius
S	fringe shift per unit fringe width
T	temperature
$u = y^2$	
$v = r^2$	
w	value of v for which density is required
x	Cartesian coordinate in direction of undeviated light ray
y	Cartesian coordinate perpendicular to light ray and to free-stream flow direction
z	zone width
γ	ratio of specific heats

κ	Gladstone-Dale constant
λ_0	wavelength of light in vacuum
v	difference between index of refraction at point r and reference index of refraction
ρ	density
ρ_{ref}	reference density
ϕ	angle between ray and normal to surface

Subscripts:

s	stagnation
0	free stream
1	unrefracted ray; also, correct value
2	refracted ray; also, approximation to correct value

APPENDIX B

ANALYSIS

The problem is to determine the density from the known fringe shift. For the two-dimensional case, where the density is not a function of x , the relation between fringe shift and density has been shown in reference 3, for example, to be

$$S = \frac{k}{\lambda_0} [\rho(y) - \rho_{\text{ref}}] L$$

For the three-dimensional case, where the density is a function also of x , the fringe shift at any point on the interferogram is the summation of the shifts produced in each element of path of the ray of light. If the assumption is made that the density distribution is axially symmetric, then ρ is a function of r alone. If the additional assumption is made that, within the disturbance, the light ray does not deviate from a straight line that is parallel to the x -axis, then the relation between fringe shift and density is

$$S = \frac{2k}{\lambda_0} \int_y^\infty [\rho(r) - \rho_{\text{ref}}] \frac{r \, dr}{\sqrt{r^2 - y^2}} \quad (1)$$

Three methods of handling equation (1) have been proposed. The earliest is that which is discussed by Schardin (reference 4). In this method, the disturbance is divided into zones, as shown in figure 10, where a zone is the region between two adjacent concentric circles. (The zone between circles i and $i + 1$, for example, is referred to in the present analysis as zone i .) The assumption is then made that the density is constant in each zone. The resulting equation, which is thus an approximation to equation (1), can be solved for $\rho(r)$.

In the second method, which was introduced by Van Voorhis (reference 1), the value of the quantity $\rho(r) - \rho_{\text{ref}}$ in each zone is assumed to be a linear function of the radius r of the zone. The resulting equation, which is thus also an approximation to equation (1), is solvable.

In the third method, which was introduced by Weyl (reference 2), equation (1) is solved exactly for $\rho(r) - \rho_{\text{ref}}$ and the resulting definite integral is approximated by assuming that in each zone the fringe shift is a linear function of y^2 . First the variables

$$v = r^2$$

$$u = y^2$$

and

$$v = \kappa [\rho(r) - \rho_{\text{ref}}]$$

are substituted into equation (1) to give the equation

$$S(u) = \frac{1}{\lambda_0} \int_u^\infty \frac{v(v) dv}{\sqrt{v-u}}$$

This integral equation is the same as Volterra's integral equation of the first kind except that the limits of integration differ from the Volterra equation limits of 0 and u . This equation can be solved in a manner similar to that used for solving Volterra's equation (references 2 and 5). The result is

$$v(w) = -\frac{\lambda_0}{\pi} \int_w^\infty \frac{S'(u) du}{\sqrt{u-w}}$$

where the prime indicates differentiation with respect to u . This resulting integral can be computed by breaking the integral into steps, one step for each zone, and by assuming that in each zone the fringe shift $S(u)$ is a linear function of u , where $r_i^2 \leq u \leq r_{i+1}^2$. Then

$$\begin{aligned} v_i &= -\frac{\lambda_0}{\pi} \left[\int_{u_i}^{u_{i+1}} \frac{S'(u) du}{\sqrt{u-u_i}} + \dots + \int_{u_k}^{u_{k+1}} \frac{S'(u) du}{\sqrt{u-u_i}} + \dots \right] \\ &= -\frac{\lambda_0}{\pi} \sum_{k=i}^{N-1} \int_{u_k}^{u_{k+1}} \frac{S_{k+1} - S_k}{\sqrt{u-u_i}} du \\ &= -\frac{2\lambda_0}{\pi} \sum_{k=i}^{N-1} \frac{S_{k+1} - S_k}{u_{k+1} - u_k} \left(\sqrt{u_{k+1} - u_i} - \sqrt{u_k - u_i} \right) \\ &= \frac{2\lambda_0}{\pi} \sum_{k=i}^{N-1} (S_k - S_{k+1}) \frac{\sqrt{r_{k+1}^2 - r_i^2} - \sqrt{r_k^2 - r_i^2}}{r_{k+1}^2 - r_k^2} \end{aligned}$$

For zones of equal width z ,

$$r_i = iz$$

and

$$v_i = \frac{2\lambda_0}{\pi z} \sum_{k=1}^{N-1} (S_k - S_{k+1}) \frac{\sqrt{(k+1)^2 - i^2} - \sqrt{k^2 - i^2}}{2k+1} \quad (2)$$

Equation (2) is an approximation to the solution of equation (1) and is the relation that was used for computing the results given in the present paper.

The coefficients

$$A_{k,i} = \frac{\sqrt{(k+1)^2 - i^2} - \sqrt{k^2 - i^2}}{2k+1}$$

for 50 zones were calculated by the Bell Telephone Laboratories X-66744 relay computer at the Langley Laboratory and are given in table I.

The situation may arise that would make desirable the use of more than 50 zones. Because the number of coefficients is approximately equal to half the square of the number of zones, a large number of coefficients would have to be calculated. A method has been devised in which the number of coefficients is equal only to the number of zones and each coefficient is also easier to calculate. The idea is to use zones not of equal width but of radius proportional to the square root of i ,

$$r = a\sqrt{i}$$

$$z = r_{i+1} - r_i$$

$$= a(\sqrt{i+1} - \sqrt{i})$$

where a is the radius of the first zone. Then

$$v_i = \frac{2\lambda_0}{\pi a} \sum_{k=1}^{N-1} (S_k - S_{k+1}) \left(\sqrt{k-i+1} - \sqrt{k-i} \right)$$

The coefficient is a function only of $k - i$, which ranges in value from 0 to $N - 1$. Therefore, only N coefficients need be calculated, rather than $N^2/2$. This new method was not used in the calculations for the present paper but is mentioned because of its possible value in future calculations.

APPENDIX C

SOURCES OF ERROR

The purpose of the present section is to consider some of the sources of error inherent in the application of equation (2). Equation (2) can be used for determining density distribution with sufficient accuracy only if the following conditions are sufficiently well satisfied:

- (a) The index of refraction of the gas varies linearly with density
- (b) A reference density at some point in the field of view of the interferometer can be determined
- (c) The disturbance is rotationally symmetrical about an axis that is known
- (d) The light beam is not refracted
- (e) The variation with y of fringe shift $S(y)$ for a cross section of the disturbance perpendicular to the axis of symmetry is known
- (f) The variation with u of fringe shift $S(u)$ can be replaced by a series of straight lines

As far as is known, condition (a) is always sufficiently well satisfied by air. Whether condition (b) is satisfied at all is generally determined by the experimental setup. For the present investigation the reference density was the free-stream density. For determining the free-stream density, the value of the stagnation temperature was measured at the instant the interferogram was taken. The Mach number given by the nozzle was known from a previous calibration described in reference 6. The free-stream temperature was then calculated from the relation

$$\frac{T_s}{T} = 1 + \frac{\gamma - 1}{2} M^2$$

Then the free-stream density was computed by the general gas law under the assumption that the free-stream static pressure was equal to the ambient atmospheric pressure, which was measured. The determination of free-stream density is, of course, subject to some degree of uncertainty. The error in free-stream density is estimated to be not greater than 3 percent, and the probable error is estimated to be about 1 percent.

Condition (c) is assumed to be satisfied for the part of the flow field that is behind the shock wave and ahead of the most upstream part of the intersection of the shock wave with the mixing region at the edges of the jet. Because the shock wave is axially symmetric and the jet is square, as soon as the shock wave reaches the edge of the jet, condition (c) is no longer satisfied.

Condition (d), that the light beam is not refracted, is usually sufficiently well satisfied in rotationally symmetric flow. (The only place the effects of refraction are likely to be large is in boundary layers in two-dimensional flow.) That the effect of refraction on fringe shift and on calculated density was fairly small in the present case was determined by calculating the effect. The purpose of the calculation was not to make a precise analysis of the effects of refraction but to determine approximately the magnitude of the effect on calculated density in the region where the effect was largest. That region is at the nose of the shock wave. Certain assumptions that greatly simplified the analysis were therefore justified. The assumption was made that the region behind the nose of the shock wave was a spherical region of constant density. When a ray of light impinges obliquely on a region of greater density, the ray is refracted and emerges at a place different from the place it would emerge if not refracted. The optical path length is, therefore, changed by the refraction. Because of the change in optical path, the fringe shift produced by the ray is also changed. Figure 11 shows the ray of light entering the sphere at P_1 and leaving at P_2 . Only a meridian plane, defined by the ray and the center of the sphere, need be considered. The geometrical path length without refraction is L_1 and with refraction is L_2 .

$$\begin{aligned} L_1 &= 2R \cos \phi_1 \\ &= 2R \sqrt{1 - \sin^2 \phi_1} \end{aligned}$$

$$\begin{aligned} L_2 &= 2R \cos \phi_2 \\ &= 2R \sqrt{1 - \sin^2 \phi_2} \end{aligned}$$

$$\sin \phi_1 = \frac{d}{R}$$

and, inasmuch as

$$n_2 \sin \phi_2 = n_1 \sin \phi_1$$

then

$$\sin \phi_2 = \frac{n_1 d}{n_2 R}$$

Therefore,

$$\left(\frac{L_2}{L_1}\right)^2 = \frac{1 - \left(\frac{n_1 d}{n_2 R}\right)^2}{1 - \left(\frac{d}{R}\right)^2}$$

The value of n_1 outside the sphere (in the free stream) is 1.0004 at Mach number 1.62. The density within the sphere is assumed to be twice that outside the sphere. Then, because $n - 1$ is proportional to the density, the value of n_2 inside the sphere is 1.0008. The ratio of n_2 to n_1 is 1.0004. The values of L_2/L_1 for various values of d/R are shown in the following table, together with the percentage error in the fringe shift. The corresponding values of distance behind the nose of the assumed sphere of constant density, expressed in terms of the distance between the nose of the shock wave and the nose of the sphere, are shown in the last column of the table.

d/R	L_2/L_1	Error in fringe shift, percent	Percent of distance from shock wave to sphere
0.995	1.039	3.9	3
.990	1.019	1.9	5
.980	1.010	1.0	11
.960	1.005	.5	22
.940	1.003	.3	32
.920	1.002	.2	43

The values of the radius of curvature of the shock wave at its nose, 2.9 times the radius of the model, and of the axial distance between the shock wave and the model, 0.56 times the radius of the model, were taken from reference 6.

The effect of refraction is seen to be small except immediately behind the shock wave. There, however, the error due to refraction may still be relatively unimportant because at the same place there may be

a larger error due to the "overshooting" in the computed density that occurs immediately behind a discontinuity in the density, such as exists at a shock wave. (The overshooting is explained subsequently in the discussion of condition (f).)

Whether condition (e) is sufficiently well satisfied for the computed value of density to lie within given limits of uncertainty depends on a number of factors. A relation that gives the effect of some of these factors is derived. Figure 10 shows a cross section of the flow field divided into concentric zones. A typical ray of light is shown traversing the field. The innermost zone through which this ray travels is designated zone 1. The assumption is then made that, for this ray, the fringe shift due to the density outside of zone 1 is accurately known. The problem is to determine how much error in the fringe shift at $y = 1$ can be tolerated for a given uncertainty in the determination of the density at the same place. Let S_{i1} be the correct value of fringe shift at $y = 1$ and S_{i2} the approximation to S_{i1} . The error in fringe shift is

$$\Delta S = S_{i1} - S_{i2}$$

From the definition of v and equation (2),

$$\begin{aligned} v_{i1} &= \kappa(\rho_1 - \rho_{\text{ref}}) \\ &= \frac{2\lambda_0}{\pi z} \sum_{k=1}^{N-1} (S_k - S_{k+1})_1 A_{k,i} \\ v_{i2} &= \kappa(\rho_2 - \rho_{\text{ref}}) \\ &= \frac{2\lambda_0}{\pi z} \sum_{k=1}^{N-1} (S_k - S_{k+1})_2 A_{k,i} \end{aligned}$$

Then, because all the fringe shifts from $k = i + 1$ to $k = N - 1$ are assumed to be accurately known and are the same for both case 1 and case 2,

$$\begin{aligned} \Delta \rho &= \rho_1 - \rho_2 \\ &= \frac{2\lambda_0}{\pi z \kappa} \Delta S A_{i,i} \end{aligned} \quad (3)$$

Equation (3) can be used to calculate the accuracy with which fringe shift must be known for determining density within specified limits.

The equation is used herein to investigate the effect of error in the value of the fringe shift on the value of the density for a sample case. A square density distribution as shown in figure 12 is assumed. The corresponding fringe-shift curve is also shown. The assumption is made that this fringe-shift curve is known to ± 0.001 . From this fringe-shift curve the density distribution is in turn recalculated. The result is the solid curve that peaks at zone 24. The overshooting that occurs at the discontinuity in density is not the result of the uncertainty of 0.001 in the fringe shift at each zone but is caused by failure of condition (f) to be satisfied and is discussed subsequently. For comparison, the assumptions are also made that the fringe shift is 0.02 too high at every zone and also that the fringe shift is 0.02 too low at every zone. The density distributions calculated under these assumptions are not shown in figure 12 since they are almost indistinguishable from each other and also from the density distribution obtained under the assumption of an uncertainty of 0.001.

Equation (3) is now applied and is found to give, at zone 15, for $\Delta S = 0.02$, a value of $\Delta \rho$ of 0.00014 slug per cubic foot. The actual value of $\Delta \rho$ is 0.00001 slug per cubic foot. For this case, therefore, equation (3) gives a very conservative estimate of the error in density.

Applying equation (3) to a case where it will give the least conservative estimate of error is desirable. The largest error in density occurs when the error in the fringe-shift curve is an oscillating one that changes sign at each zone. The density distribution obtained under this assumption of fringe-shift error is shown by the oscillating curve in figure 12 for $|\Delta S| = 0.02$. At zone 15 the error in density is 0.0001 slug per cubic foot. This value is to be compared with the value 0.00014 slug per cubic foot calculated by equation (3). Equation (3), therefore, appears to be a good approximation in this case, which is one that simulates those that occur in actual practice.

Satisfying condition (e), that is, obtaining fringe shift with sufficient accuracy, is perhaps the most difficult requirement to meet in obtaining density distributions in three-dimensional flows. Because equation (3) so clearly illustrates the difficulty, the equation is used in another example to show how accurately the fringe shifts must be known for the density to be determined accurately. A typical position in figure 5(b) is chosen and the requirement is made that the density be obtained within 1 percent. A position is chosen about midway

along the contour on which the ratio of density to free-stream density is 2.0. For this position,

$$\lambda_0 = 5.17 \times 10^{-5} \text{ centimeters}$$

$$z = 2.3 \times 10^{-2} \text{ centimeters}$$

$$\kappa = 0.1167 \text{ cubic foot per slug}$$

$$i = 24$$

$$A_{i,i} = 0.14$$

$$\rho = 0.0070 \text{ slug per cubic foot}$$

$$\Delta\rho = 0.00007 \text{ slug per cubic foot}$$

Then, by equation (3),

$$\Delta S = 0.04$$

In the present investigation, fringe shifts could generally be determined with approximately twice this amount of uncertainty, or ΔS approximately equal to 0.1, for the interferogram of the flow at Mach number 1.62. For the interferogram taken at Mach number 1.30, however the fringe shifts were somewhat more uncertain than for the other interferogram. The model is farther from the end of the nozzle, and turbulence in the mixing regions on the two sides of the jet through which the light passes causes appreciable irregularities in the fringe pattern.

That the effect of shrinkage of the film during development was negligibly small was found by photographing a transparent scale. Furthermore, by enlarging photographs of a scale, it was found that distortions introduced by the lens of the enlarger were also negligibly small.

Condition (f) is that $S(u)$ can be replaced by a straight line in each zone. Weyl has shown (reference 2) that this condition is sufficiently well satisfied everywhere except in zones in which the rate of change of $S'(u)$ is large, that is, where the second derivative of $S(u)$ has large absolute values. At shock waves the second derivative of $S(u)$ is very large. The result is that condition (f) is grossly violated and the calculated density overshoots at shock waves. At other places where the second derivative is large, but not so large as at shock waves, condition (f) can, by the use of smaller zone widths, generally be sufficiently well satisfied in that the error due to violation of condition (f) is acceptably small.

APPENDIX D

COMPUTATIONAL PROCEDURE

The negatives of the interferograms were about $1\frac{1}{2}$ inches in diameter. Prints were made in which the negatives were enlarged about 16 diameters and these prints were used for all measurements.

The computational procedure used is as follows:

The axis of symmetry was drawn on each interferogram. On each no-flow interferogram the fringes were numbered arbitrarily. A cross section was drawn perpendicular to the axis of symmetry and the position of each fringe was measured along the cross section. Then fringe number was plotted as a function of position. A large scale that will permit reading the curve with the required accuracy had to be used.

On the flow interferograms, lines perpendicular to the axis of symmetry were drawn. These lines were spaced about 1/10 inch apart and denoted the cross sections along each of which the fringe shift was to be measured. Again the fringes were arbitrarily numbered and the positions of the fringes were measured along each cross section. The positions of both the black and the white fringes were measured, because on part of the interferogram the fringes run almost parallel to the cross sections and the number of points is, therefore, less than is desirable.

The next step was to determine the fringe shift at each measured point on each cross section. The position of each fringe is known. The position of the disturbed fringe was used in the previously mentioned plot of fringe number as a function of fringe position to determine the number of the undisturbed fringe at that position. Then the number of the undisturbed fringe was subtracted from the number of the disturbed fringe to give the fringe shift.

Because the fringes had been arbitrarily numbered, all fringe shifts were adjusted by the amount necessary to make the undisturbed fringe at the same location in both flow and no-flow interferograms have the same number. This adjustment is tantamount to numbering the fringes on either the flow or the no-flow interferogram not arbitrarily but in such a way that the same number is given to the same position in the undisturbed portion of both interferograms.

Because the free-stream density was to be used as the reference density in computing density distribution around the sphere and because the fringe shift must be assumed to be zero for the reference density,

the fringe shift in the free stream had to be determined and subtracted from all other fringe shifts. The fringe shift in the free stream was determined from the free-stream density which was calculated as described in appendix C.

A cross section in the free stream was chosen as giving the positions of the reference fringes. The fringes in the free stream were at a slight angle to the axis and, therefore, to the cross sections which were drawn perpendicular to the axis. This tilt of the free-stream fringes has an effect on the fringe shifts measured along each cross section in that it causes them to be different by an amount that is proportional to the tangent of the angle of tilt and to the distance of the cross section from the reference cross section. Proper adjustment of the measured fringe shifts along each cross section was made to eliminate the effect of the tilt.

The next step was to plot fringe shift as a function of position. Here again, care must be taken to use a sufficiently large scale. The plot was then divided into zones, with the zeroth zone at the axis of symmetry. Zone width is generally determined by a number of factors. Equation (3) shows that the greater the zone width the less the error in density due to violation of condition (e). On the other hand, the greater the zone width, the smaller the number of zones, the less well condition (f) is satisfied, and the smaller the number of experimental points that will be obtained. A compromise in zone width is, therefore, necessary. For the present investigation, the cross sections were separated into groups of nine each. The same zone width was used for all cross sections in a group and was such that the longest cross section in each group was divided into 50 zones.

The next step was to read the fringe shift at each zone and then to determine, by subtracting, the change in fringe shift between adjacent zones. This last quantity is the quantity $S_k - S_{k+1}$ that is used in equation (2) for calculating ν . The computations were made by the Bell computer. From the values of ν the values of the ratio of the density to the free-stream density were computed. These values were used to obtain a plot of the density ratio against zone number for each cross section. A typical plot is shown in figure 13, which is for a cross section that is about three-fourths of the way between the nose of the shock wave and the nose of the sphere.

The plot for each cross section has two regions where the inaccuracy or uncertainty is greater than for the rest of the curve. One of these regions is at and near the shock wave. There the inaccuracy is caused by failure to satisfy condition (f), and the result is overshooting or undershooting at the shock wave. (In fig. 13 the shock wave is at zone 43 and the correct density ratio behind the shock wave is 1.77.)

The density ratio across a shock wave is known, however, from well-established theory. The correct values of the density ratio behind the shock wave, therefore, can be shown on the plots of density ratio. The other region of relatively large inaccuracy is at and near the axis of symmetry (zones 0 to 5 in fig. 13). That the region of the axis is a region of relatively large inaccuracy can be seen from equation (3), which shows that the uncertainty in density is proportional to the coefficient $A_{1,i}$. The coefficient $A_{1,i}$ can be seen from table I to be larger for zone 0, which is at the axis of symmetry, than for any other zone. Unlike the other region of relatively large inaccuracy, however, for which the density ratio immediately behind the shock wave is known, the density-ratio distribution along the axis of symmetry is not known from theory.

REFERENCES

1. Ladenburg, R., Van Voorhis, C. C., and Winckler, J.: Interferometric Study of Supersonic Phenomena. Part I: A Supersonic Air Jet at 60 LB/IN² Tank Pressure. NAVORD Rep. 69-46, Bur. Ordnance, Navy Dept., April 17, 1946; Part II: The Gas Flow around Various Objects in a Free Homogeneous Supersonic Air Stream. NAVORD Rep. 93-46, Sept. 2, 1946.
2. Weyl, F. Joachim: Analytical Methods in Optical Examination of Supersonic Flow. NAVORD Rep. 211-45, Bur. Ordnance, Navy Dept., Dec. 11, 1945.
3. Gooderum, Paul B., Wood, George P., and Brevoort, Maurice J.: Investigation with an Interferometer of the Turbulent Mixing of a Free Supersonic Jet. NACA Rep. 963, 1950.
4. Schardin, H.: Theory and Applications of the Mach-Zehnder Interference-Refractometer. Univ. Texas, Defense Res. Lab., 1946.
5. Margenau, Henry, and Murphy, George Moseley: The Mathematics of Physics and Chemistry. D. Van Nostrand Co., Inc., 1943, pp. 506-507.
6. Heberle, Juergen W., Wood, George P., and Gooderum, Paul B.: Data on Shape and Location of Detached Shock Waves on Cones and Spheres. NACA TN 2000, 1950.

TABLE I.- COEFFICIENTS $A_{k,1}$ - Continued

11	0.20851																		
12	.085295	0.20000																	
13	.064150	.081893	0.19245																
14	.053027	.061686	.078868	0.18570															
15	.045836	.051065	.059486	.076155	0.17961														
16	.040683	.044199	.049305	.057506	.073704	0.17408													
17	.036752	.039281	.042727	.047716	.055711	.071476	0.16903												
18	.033625	.035527	.038014	.041392	.046271	.054074	.069438	0.16440											
19	.031061	.032541	.034417	.036862	.040176	.044950	.052574	.067565	0.16013										
20	.028909	.030090	.031555	.033405	.035809	.039060	.043736	.051192	.065836	0.15617									
21	.027070	.028033	.029205	.030653	.032478	.034842	.038033	.042615	.049913	.064233									
22	.025477	.026274	.027232	.028394	.029825	.031623	.033949	.037082	.041576	.048726									
23	.024079	.024749	.025544	.026496	.027647	.029060	.030833	.033121	.036200	.040610									
24	.022841	.023410	.024080	.024872	.025817	.026956	.028352	.030099	.032351	.035378									
25	.021735	.022224	.022794	.023462	.024250	.025187	.026314	.027692	.029415	.031632									
26	.020740	.021163	.021654	.022224	.022890	.023673	.024601	.025716	.027077	.028776									
27	.019839	.020208	.020634	.021126	.021695	.022358	.023135	.024055	.025157	.026501									
28	.019018	.019343	.019715	.020143	.020635	.021202	.021861	.022632	.023543	.024633									
29	.018267	.018554	.018882	.019257	.019685	.020176	.020741	.021396	.022161	.023062									
30	.017577	.017832	.018123	.018453	.018829	.019257	.019747	.020309	.020959	.021717									
31	.016940	.017168	.017427	.017720	.018052	.018428	.018856	.019344	.019903	.020548									
32	.016350	.016555	.016786	.017048	.017343	.017676	.018052	.018479	.018964	.019520									
33	.015802	.015987	.016195	.016429	.016693	.016989	.017322	.017698	.018123	.018607									
34	.015291	.015458	.015646	.015857	.016094	.016359	.016656	.016989	.017364	.017788									
35	.014814	.014966	.015136	.015327	.015540	.015778	.016044	.016342	.016675	.017049									
36	.014367	.014505	.014660	.014833	.015026	.015241	.015481	.015747	.016045	.016377									
37	.013947	.014073	.014215	.014373	.014548	.014743	.014959	.015199	.015466	.015763									
38	.013552	.013668	.013798	.013942	.014102	.014279	.014475	.014692	.014932	.015199									
39	.013180	.013286	.013405	.013537	.013683	.013845	.014024	.014221	.014439	.014679									
40	.012828	.012926	.013036	.013157	.013291	.013439	.013602	.013782	.013980	.014198									
41	.012495	.012586	.012687	.012799	.012922	.013058	.013207	.013372	.013552	.013751									
42	.012180	.012264	.012357	.012460	.012574	.012699	.012837	.012987	.013152	.013334									
43	.011880	.011958	.012045	.012140	.012246	.012361	.012487	.012626	.012778	.012944									
44	.011596	.011668	.011749	.011837	.011934	.012041	.012158	.012286	.012426	.012578									
45	.011325	.011392	.011467	.011549	.011640	.011739	.011847	.011965	.012094	.012235									
46	.011067	.011130	.011199	.011276	.011360	.011452	.011552	.011662	.011781	.011911									
47	.010821	.010879	.010944	.011016	.011094	.011180	.011273	.011375	.011485	.011605									
48	.010585	.010640	.010701	.010768	.010841	.010921	.011008	.011102	.011205	.011316									
49	.010360	.010412	.010468	.010531	.010599	.010674	.010755	.010843	.010939	.011043									
50	.010149	.010188	.010248	.010307	.010366	.010436	.010515	.010594	.010693	.010782									
k	1	11	12	13	14	15	16	17	18	19	20								

TABLE I.- COEFFICIENTS $A_{k,1}$ - Continued

21	0.15250										
22	.062742	0.14907									
23	.047620	.061350	0.14586								
24	.039708	.046585	.060047	0.14286							
25	.034609	.038864	.045616	.058824	0.14003						
26	.030959	.033888	.038071	.044704	.057672	0.13736					
27	.028176	.030328	.033211	.037325	.043845	.056585	0.13484				
28	.025960	.027613	.029733	.032572	.036621	.043034	.055558	0.13245			
29	.024141	.025452	.027082	.029173	.031969	.035956	.042266	.054585	0.13019		
30	.022610	.023676	.024971	.026581	.028642	.031399	.035325	.041538	.053661	0.12804	
31	.021300	.022184	.023238	.024517	.026106	.028140	.030857	.034727	.040846	.052782	
32	.020161	.020905	.021780	.022823	.024087	.025656	.027663	.030343	.034158	.040188	
33	.019159	.019794	.020532	.021398	.022430	.023679	.025229	.027210	.029854	.033616	
34	.018268	.018817	.019447	.020178	.021036	.022056	.023291	.024822	.026778	.029388	
35	.017470	.017948	.018492	.019117	.019842	.020691	.021700	.022921	.024434	.026366	
36	.016749	.017169	.017644	.018184	.018804	.019522	.020362	.021361	.022569	.024064	
37	.016095	.016466	.016883	.017354	.017891	.018506	.019217	.020049	.021037	.022232	
38	.015496	.015826	.016196	.016611	.017079	.017611	.018221	.018926	.019750	.020728	
39	.014946	.015242	.015571	.015939	.016351	.016816	.017345	.017949	.018647	.019464	
40	.014439	.014705	.015000	.015328	.015693	.016103	.016565	.017090	.017689	.018381	
41	.013969	.014210	.014475	.014769	.015095	.015459	.015867	.016325	.016845	.017440	
42	.013532	.013751	.013991	.014256	.014549	.014873	.015235	.015640	.016095	.016611	
43	.013125	.013324	.013543	.013782	.014046	.014338	.014661	.015021	.015423	.015875	
44	.012745	.012926	.013125	.013343	.013582	.013846	.014136	.014457	.014815	.015214	
45	.012387	.012554	.012736	.012935	.013153	.013391	.013653	.013942	.014262	.014617	
46	.012052	.012205	.012372	.012554	.012753	.012970	.013208	.013469	.013756	.014074	
47	.011736	.011877	.012031	.012198	.012380	.012578	.012795	.013032	.013292	.013578	
48	.011437	.011568	.011710	.011864	.012031	.012213	.012411	.012626	.012862	.013121	
49	.011155	.011276	.011407	.011549	.011704	.011871	.012052	.012249	.012464	.012700	
50	.010891	.011000	.011119	.011257	.011396	.011554	.011723	.011891	.012089	.012307	
k	1	21	22	23	24	25	26	27	28	29	30

TABLE I.- COEFFICIENTS $A_{k,1}$ - Continued

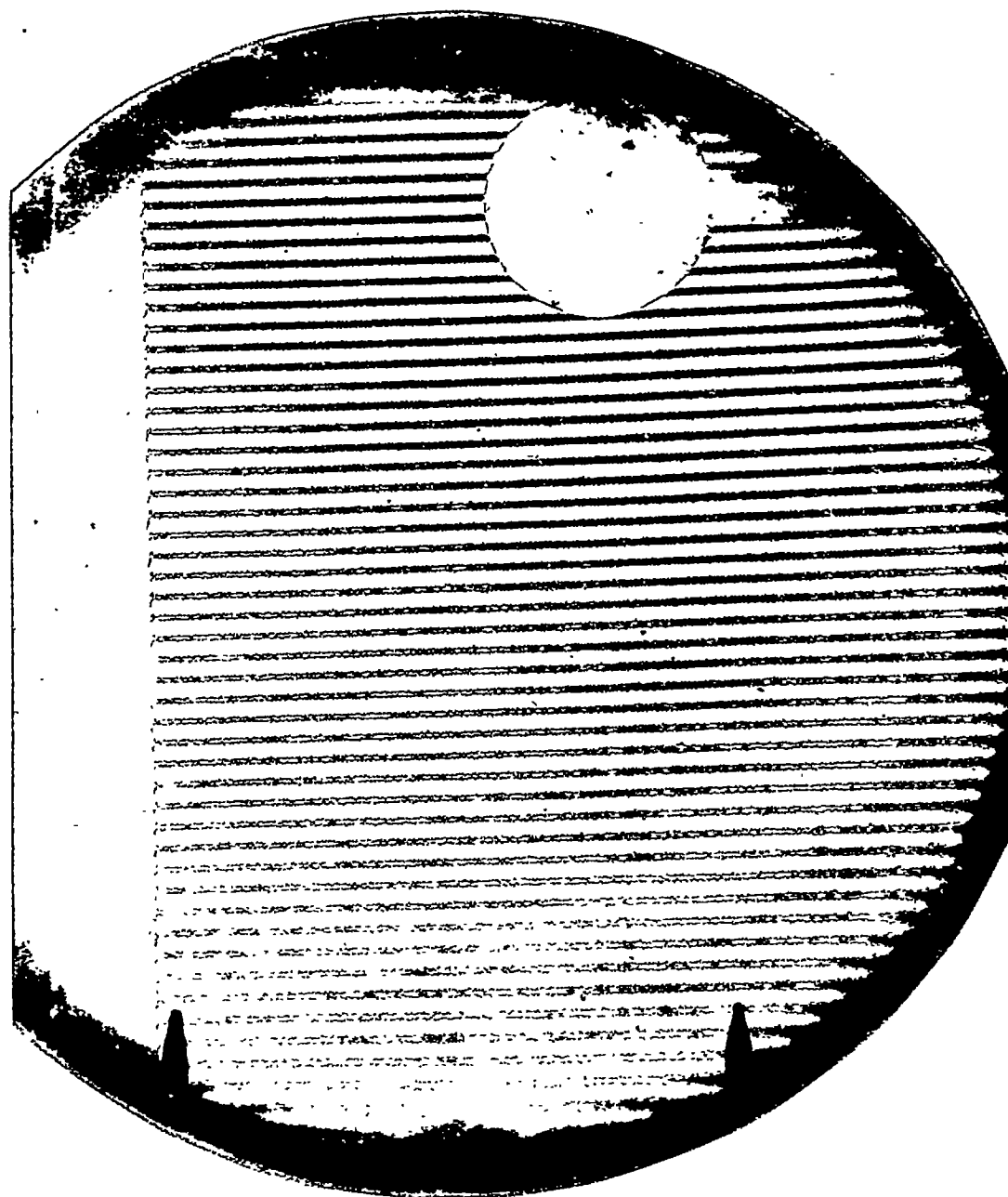
31	0.12599										
32	.051945	0.12404									
33	.039560	.051147	0.12217								
34	.033099	.038961	.050385	0.12039							
35	.028943	.032605	.038389	.049655	0.11868						
36	.025973	.028517	.032133	.037841	.048957	0.11704					
37	.023710	.025596	.028110	.031681	.037315	.048287	0.11547				
38	.021910	.023371	.025236	.027720	.031247	.036811	.047644	0.11396			
39	.020432	.021601	.023047	.024890	.027345	.030830	.036327	.047026	0.11251		
40	.019190	.020148	.021305	.022735	.024559	.026985	.030430	.035862	.046431	0.11111	
41	.018126	.018927	.019876	.021021	.022436	.024240	.026640	.030045	.035414	.045858	
42	.017201	.017881	.018675	.019614	.020748	.022149	.023933	.026307	.029674	.034982	
43	.016387	.016972	.017646	.018432	.019363	.020486	.021872	.023537	.025986	.029317	
44	.015663	.016171	.016751	.017419	.018199	.019121	.020233	.021605	.023353	.025677	
45	.015014	.015460	.015964	.016539	.017202	.017974	.018888	.019989	.021348	.023078	
46	.014427	.014822	.015264	.015764	.016335	.016992	.017758	.018663	.019754	.021100	
47	.013894	.014245	.014636	.015076	.015572	.016138	.016790	.017549	.018446	.019527	
48	.013406	.013720	.014069	.014458	.014894	.015387	.015948	.016594	.017347	.018236	
49	.012957	.013240	.013553	.013899	.014286	.014719	.015208	.015765	.016406	.017152	
50	.012545	.012792	.013079	.013386	.013733	.014119	.014554	.015035	.015584	.016224	
k	1	31	32	33	34	35	36	37	38	39	40

NACA

TABLE I.- COEFFICIENTS $A_{k,1}$ - Concluded

k1	0.10976									
k2	.045306	0.10847								
k3	.034566	.044774	0.10721							
k4	.028972	.034164	.044260	0.10600						
k5	.025378	.028639	.033776	.043763	0.10483					
k6	.022813	.025090	.028318	.033401	.043282	0.10370				
k7	.020860	.022557	.024811	.028007	.033038	.042817	0.10260			
k8	.019308	.020628	.022309	.024542	.027705	.032687	.042367	0.10153		
k9	.018034	.019096	.020404	.022069	.024281	.027414	.032347	.041931	0.10050	
50	.016970	.017838	.018890	.020188	.021837	.024028	.027129	.032017	.041506	0.099504
k1	k1	k2	k3	k4	k5	k6	k7	k8	k9	50

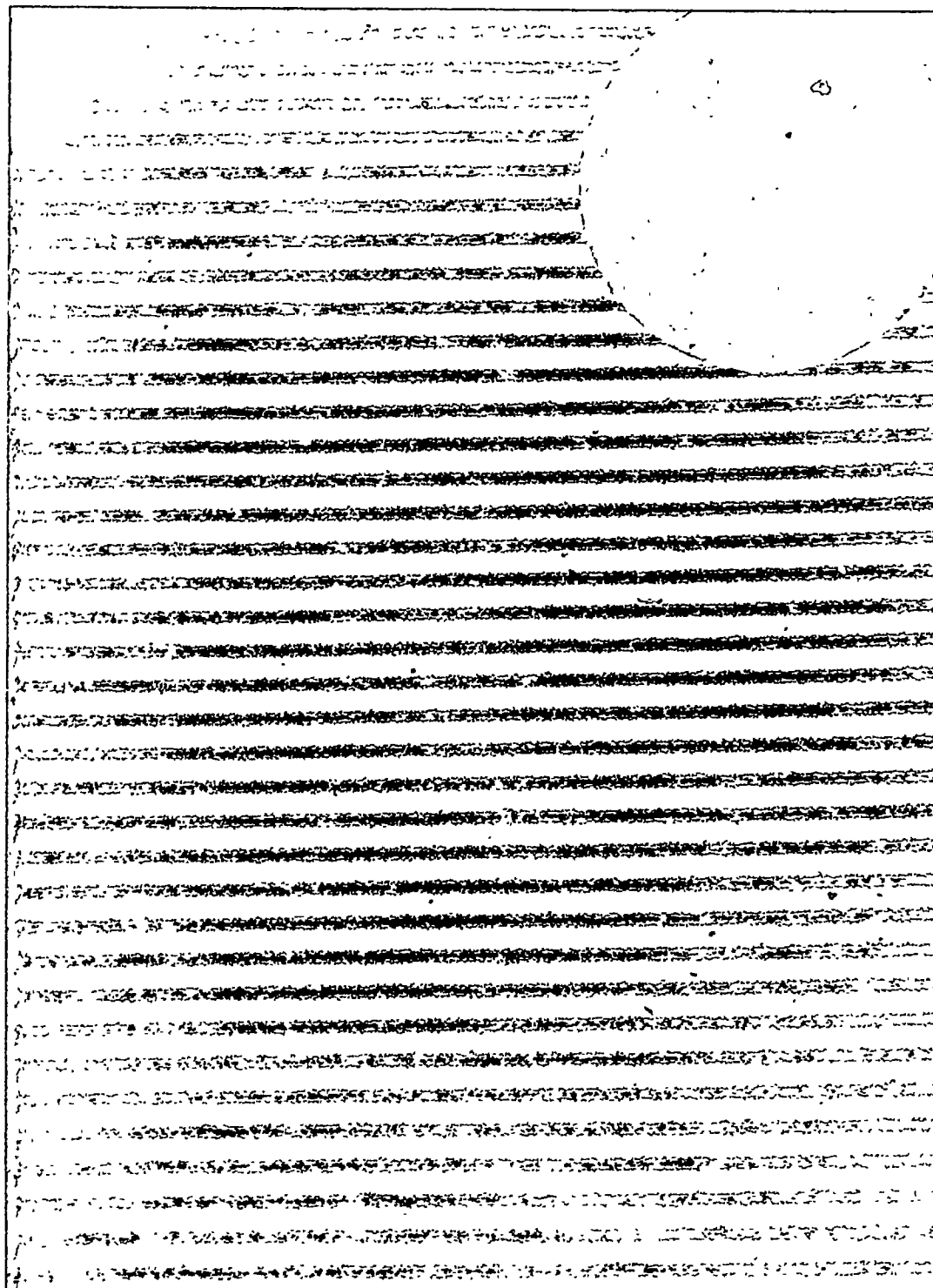
NACA



(a) Full field of view.

NACA
L-64895

Figure 1.- Undisturbed fringes for analyzing interferogram of flow at
Mach number 1.30.



(b) Region used in analysis.

NACA
L-64896

Figure 1.- Concluded.



(a) Full field of view.



L-64897

Figure 2.- Interferogram of flow around sphere at Mach number 1.30.



(b) Region used in analysis.


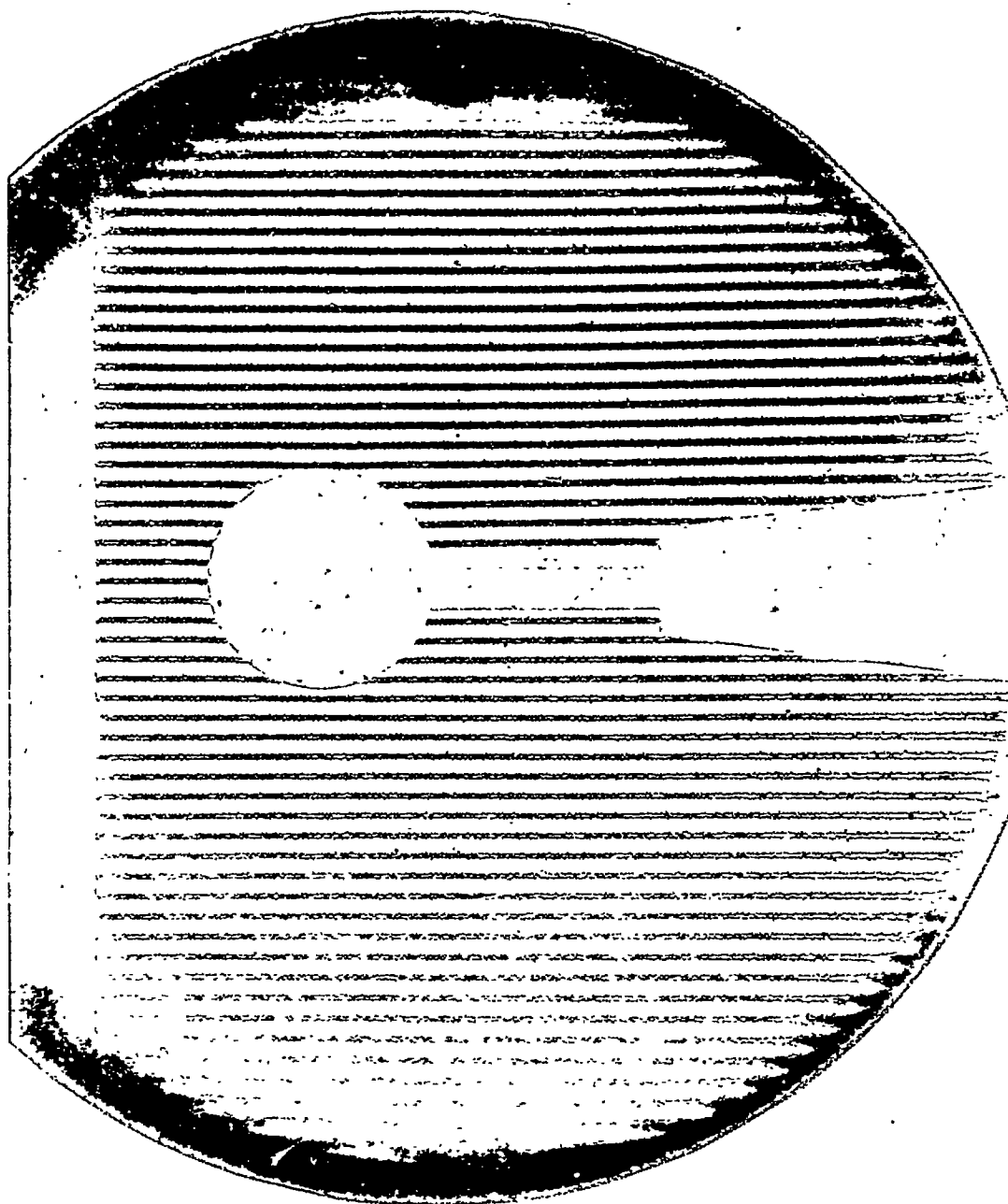

L-64898

Figure 2.- Concluded.



(a) Full field of view.


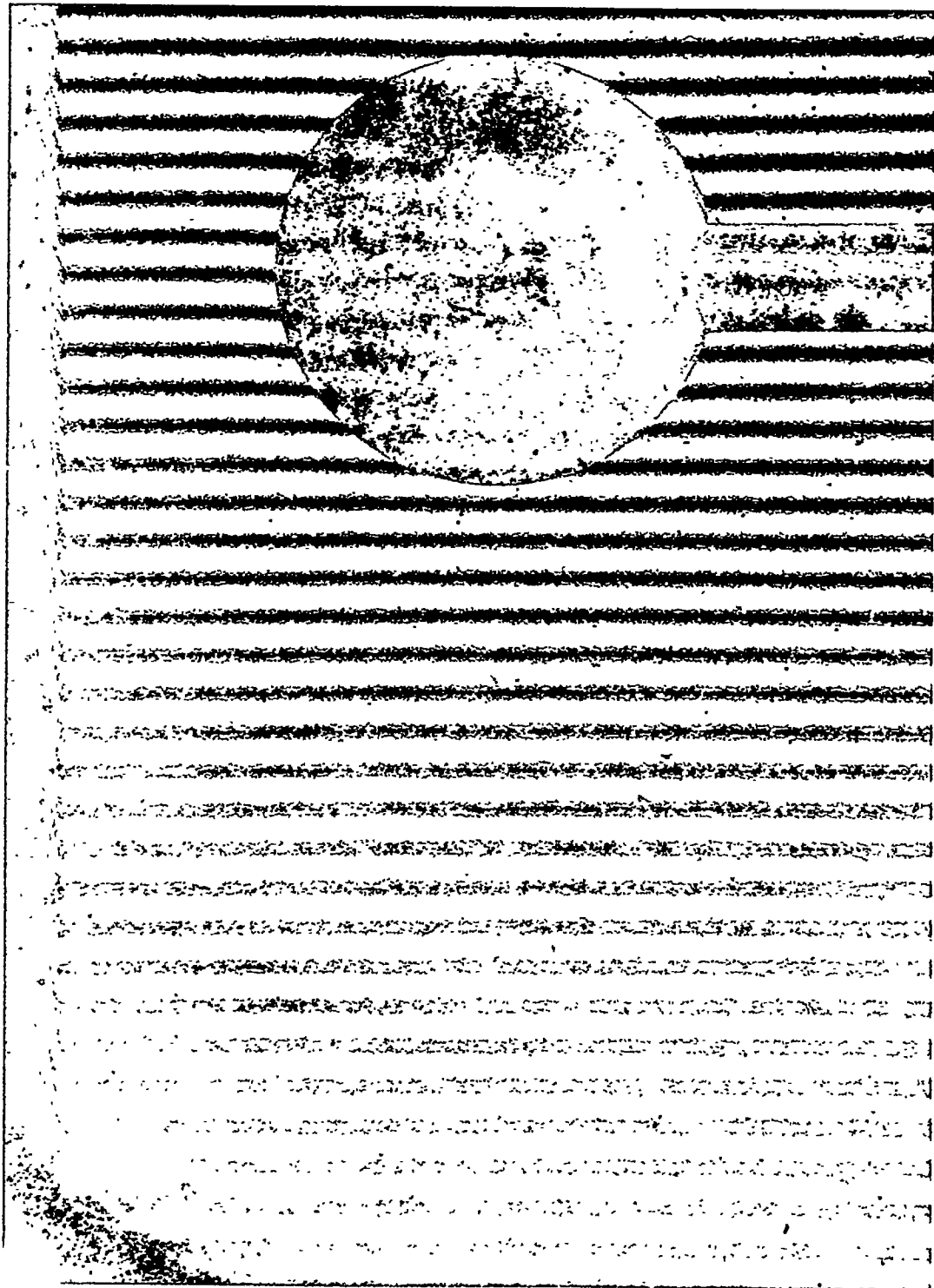

L-64899

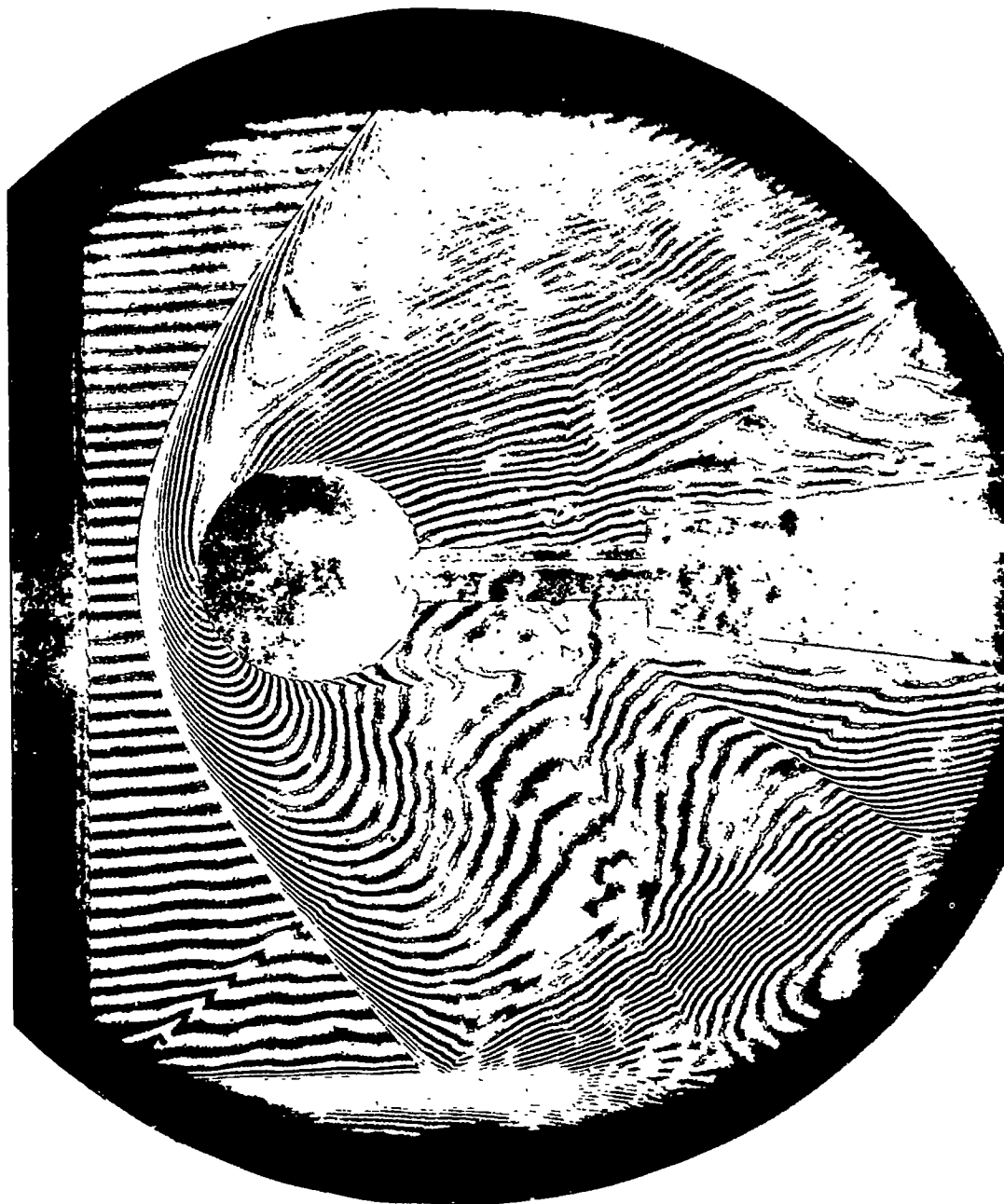
Figure 3.- Undisturbed fringes for analyzing interferogram of flow at
Mach number 1.62.



(b) Region used in analysis.

NACA
L-64900

Figure 3.- Concluded.



(a) Full field of view.



L-64901

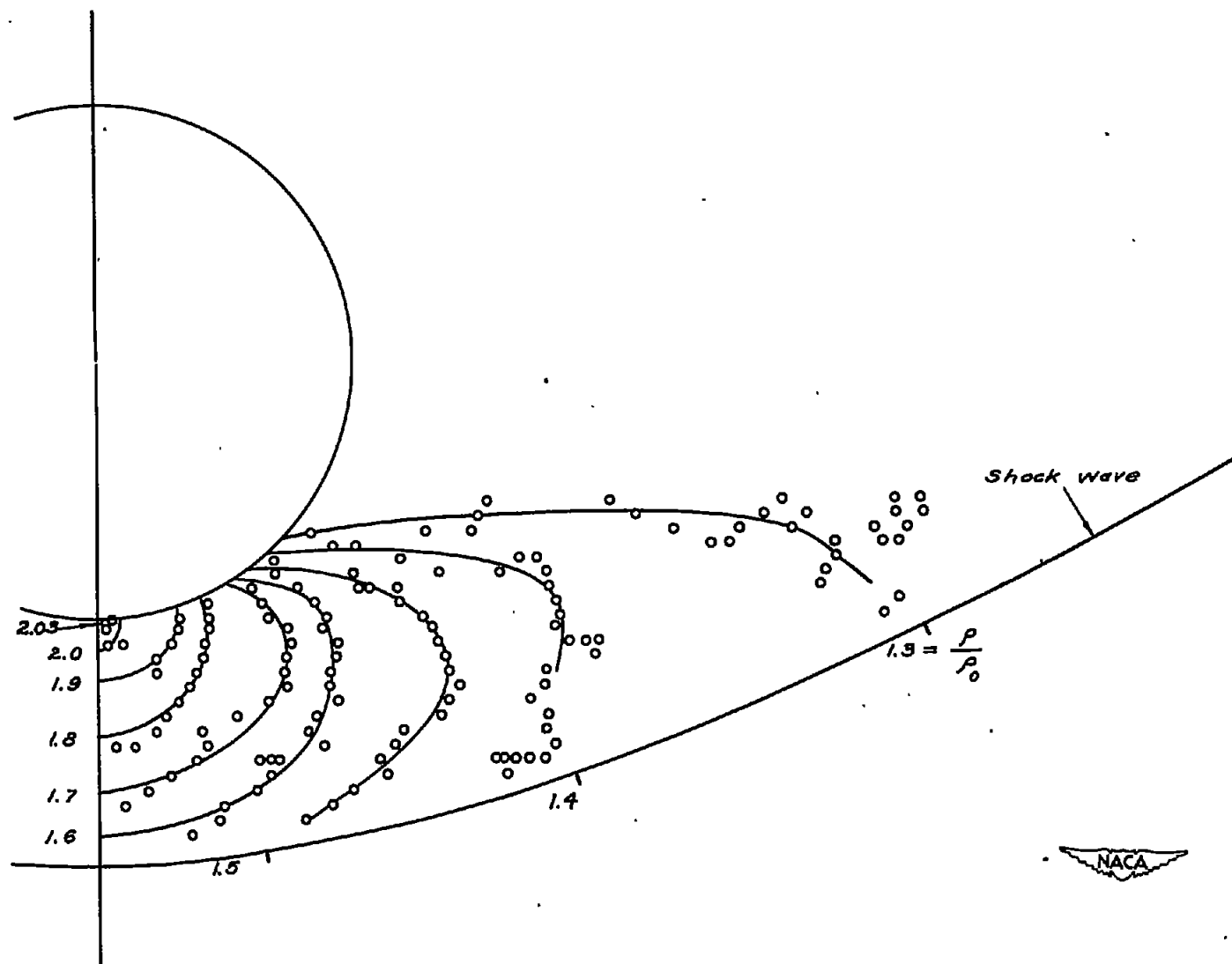
Figure 4.- Interferogram of flow around sphere at Mach number 1.62.



(b) Region used in analysis.

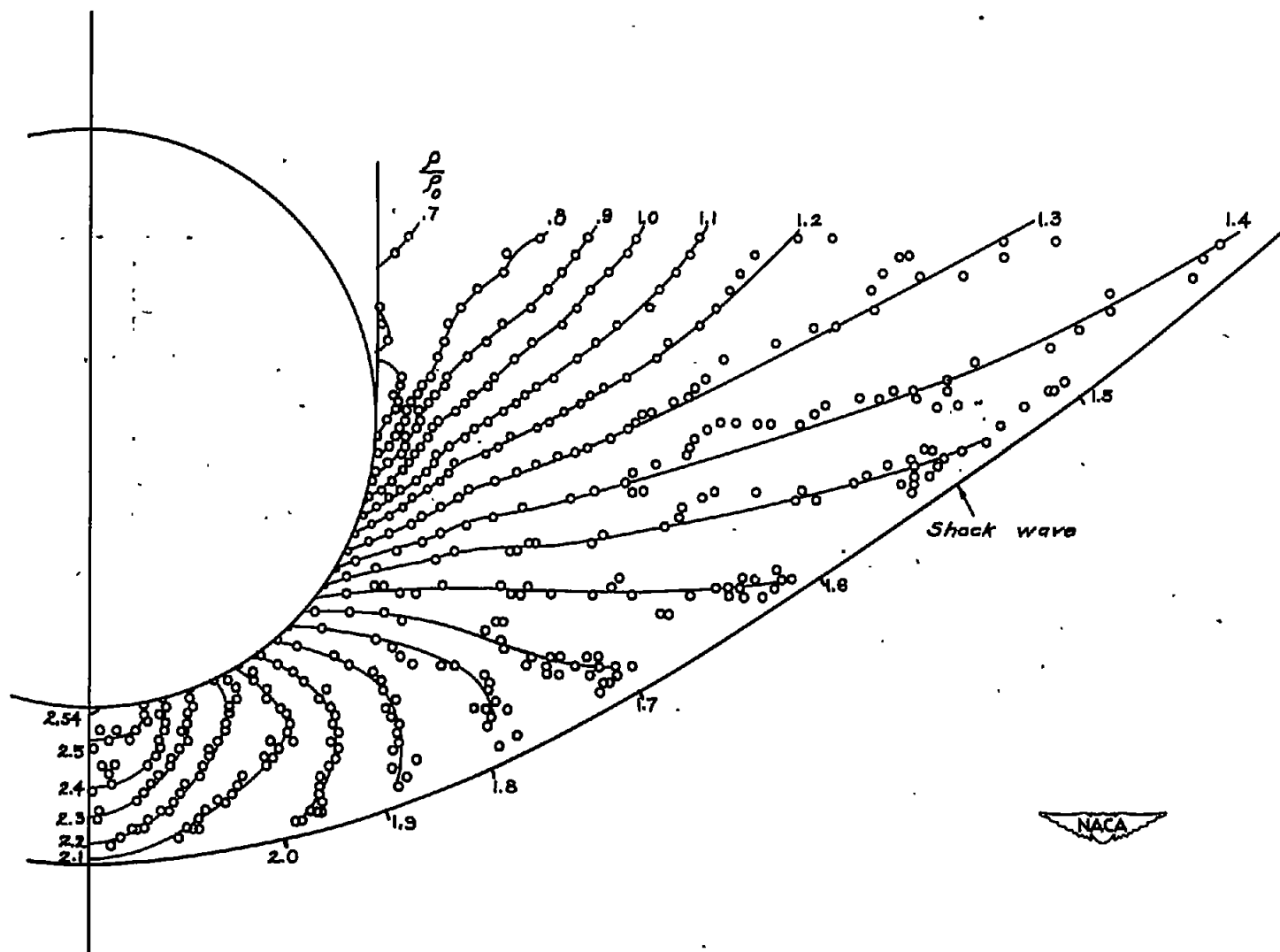
Figure 4.- Concluded.

NACA
L-64902



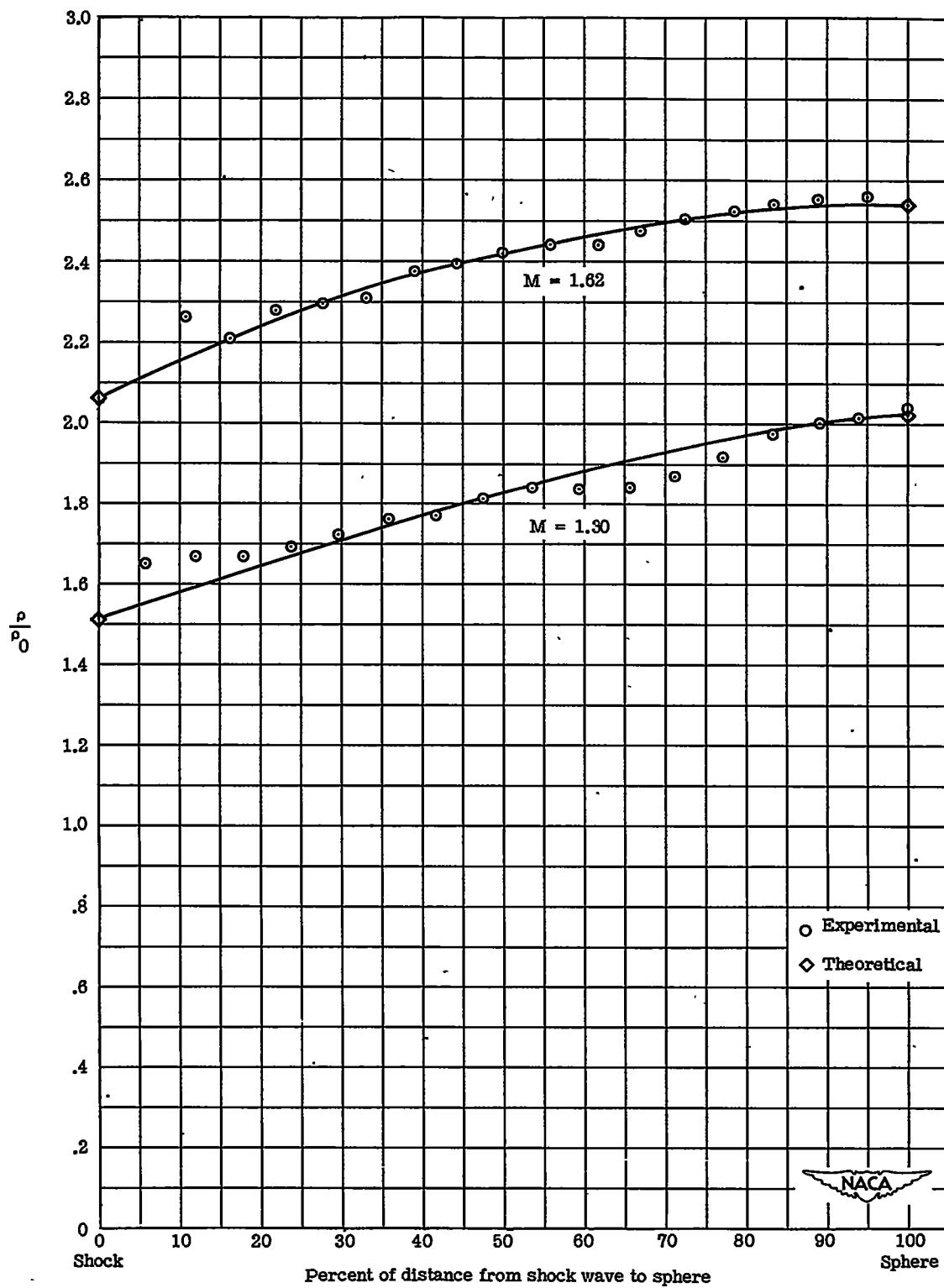
(a) $M = 1.30$.

Figure 5.- Contours of constant ratio of density to free-stream density.



(b) $M = 1.62$.

Figure 5.- Concluded.

Figure 6.- Variation along axis of ratio ρ/ρ_0 .

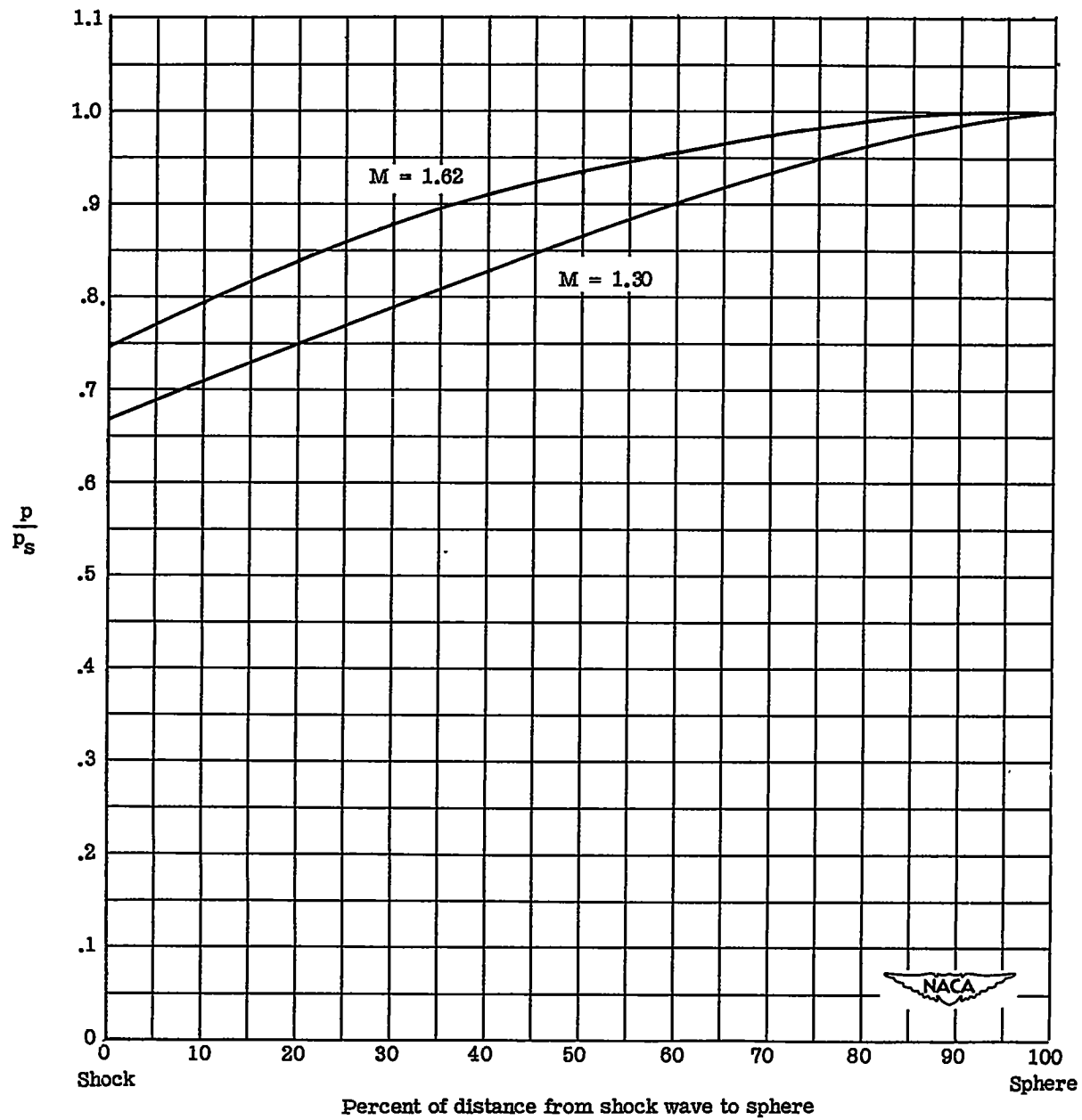


Figure 7.- Variation along axis of ratio p/p_s .

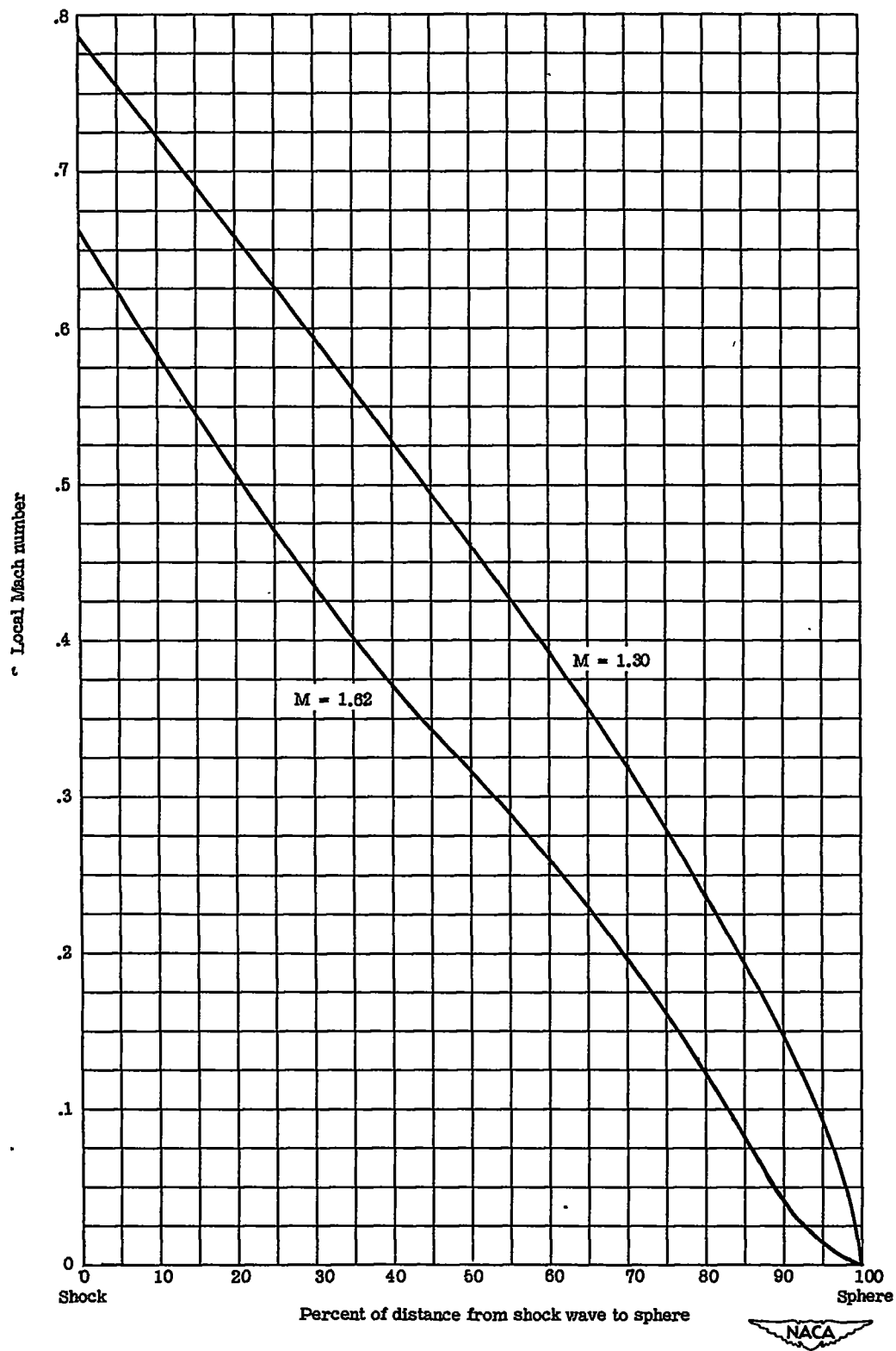


Figure 8.- Variation along axis of local Mach number.

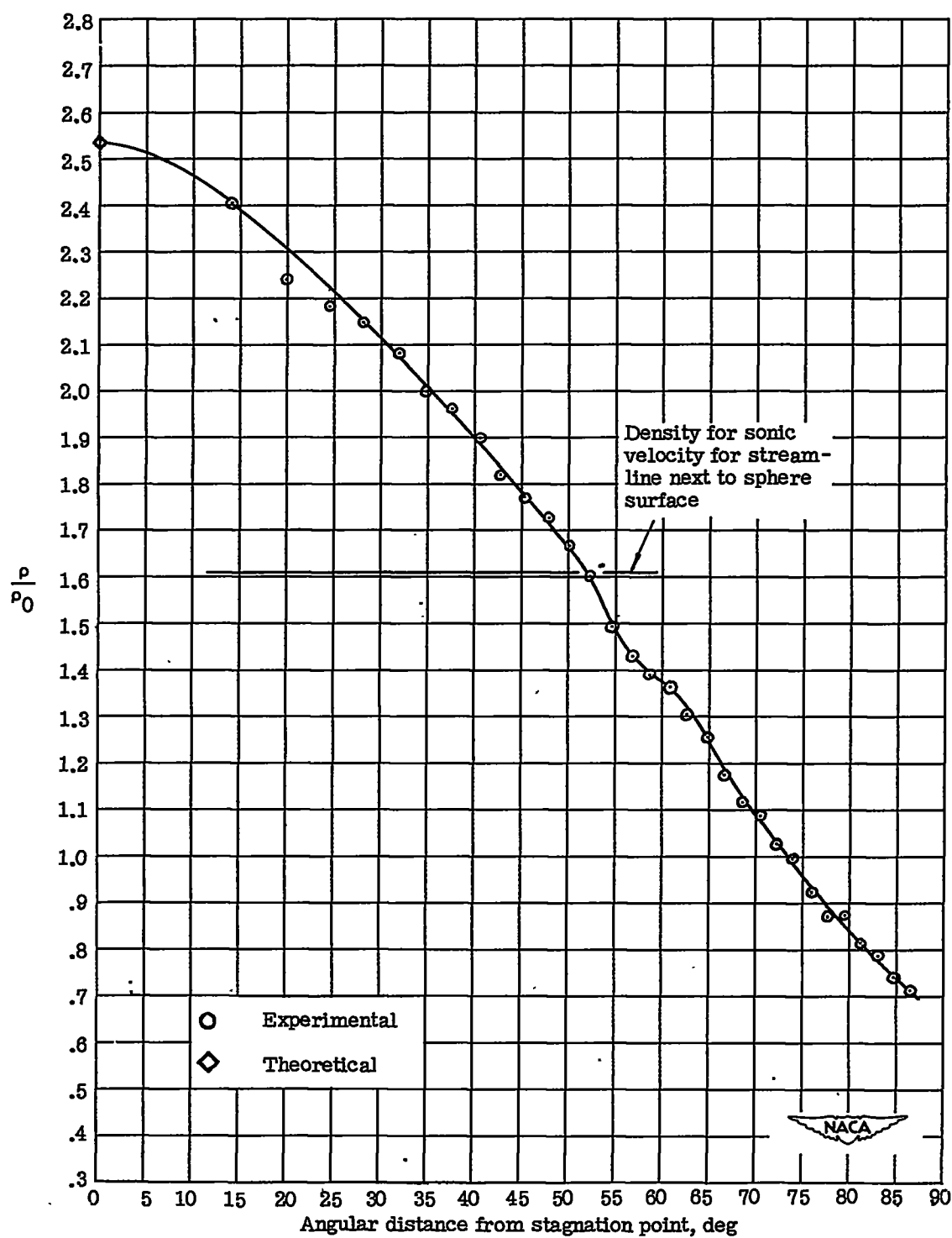


Figure 9.- Variation of the density ratio ρ/ρ_0 with angular distance from the stagnation point along the surface of the sphere. $M = 1.62$.

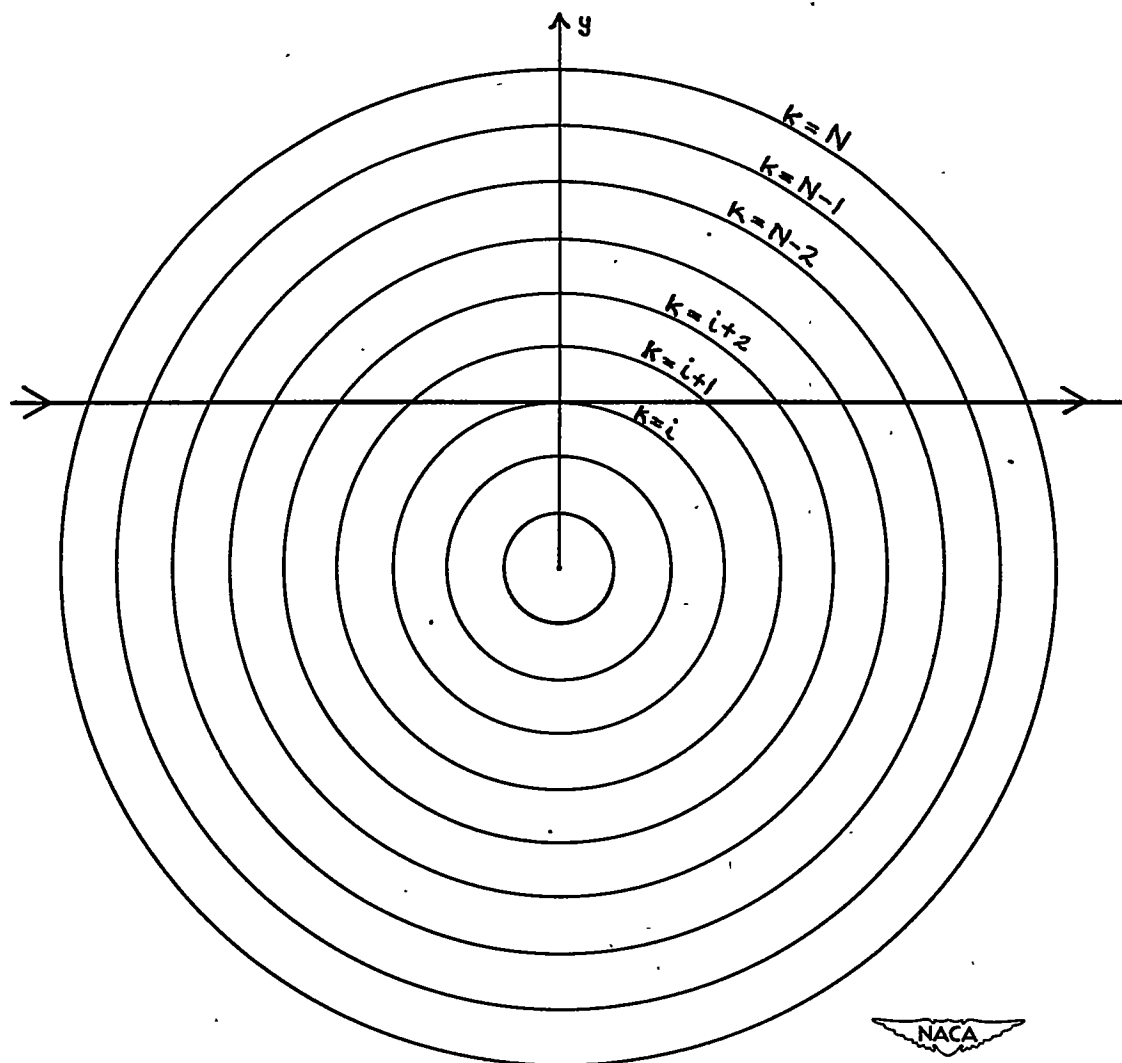


Figure 10.- Concentric zones in disturbance.

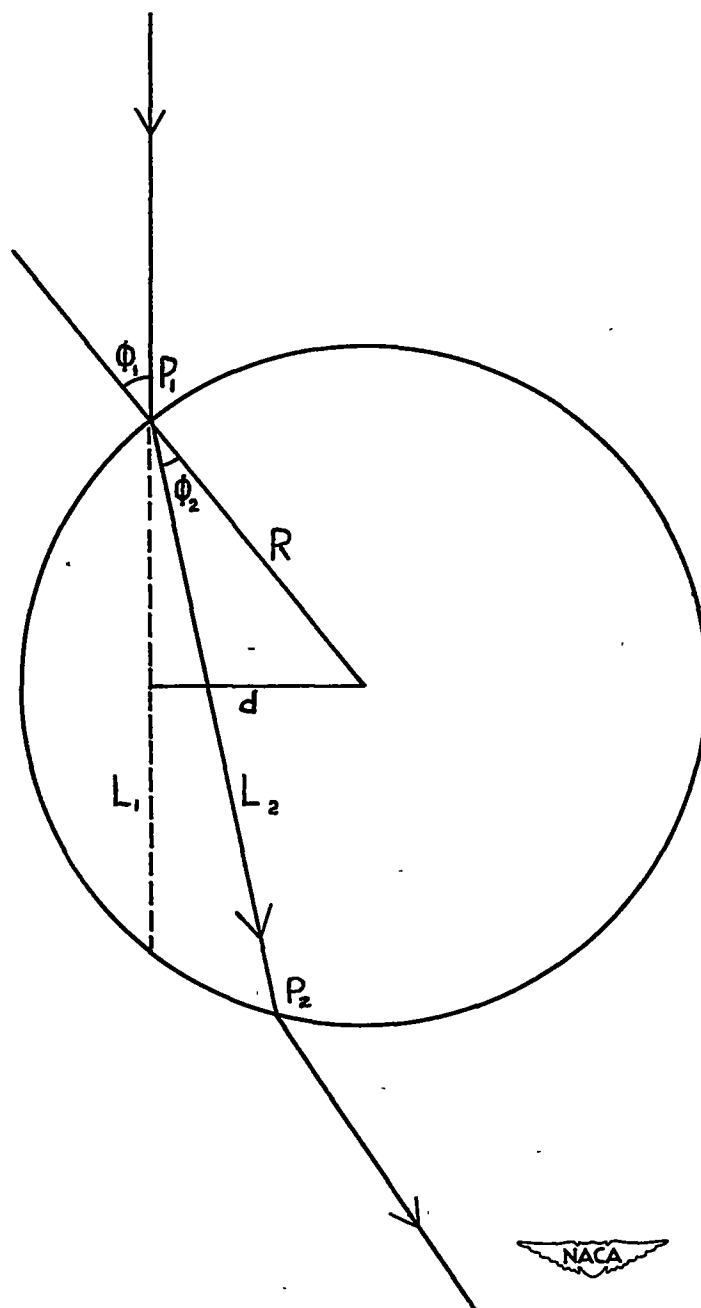


Figure 11.- Refraction of light ray by sphere.

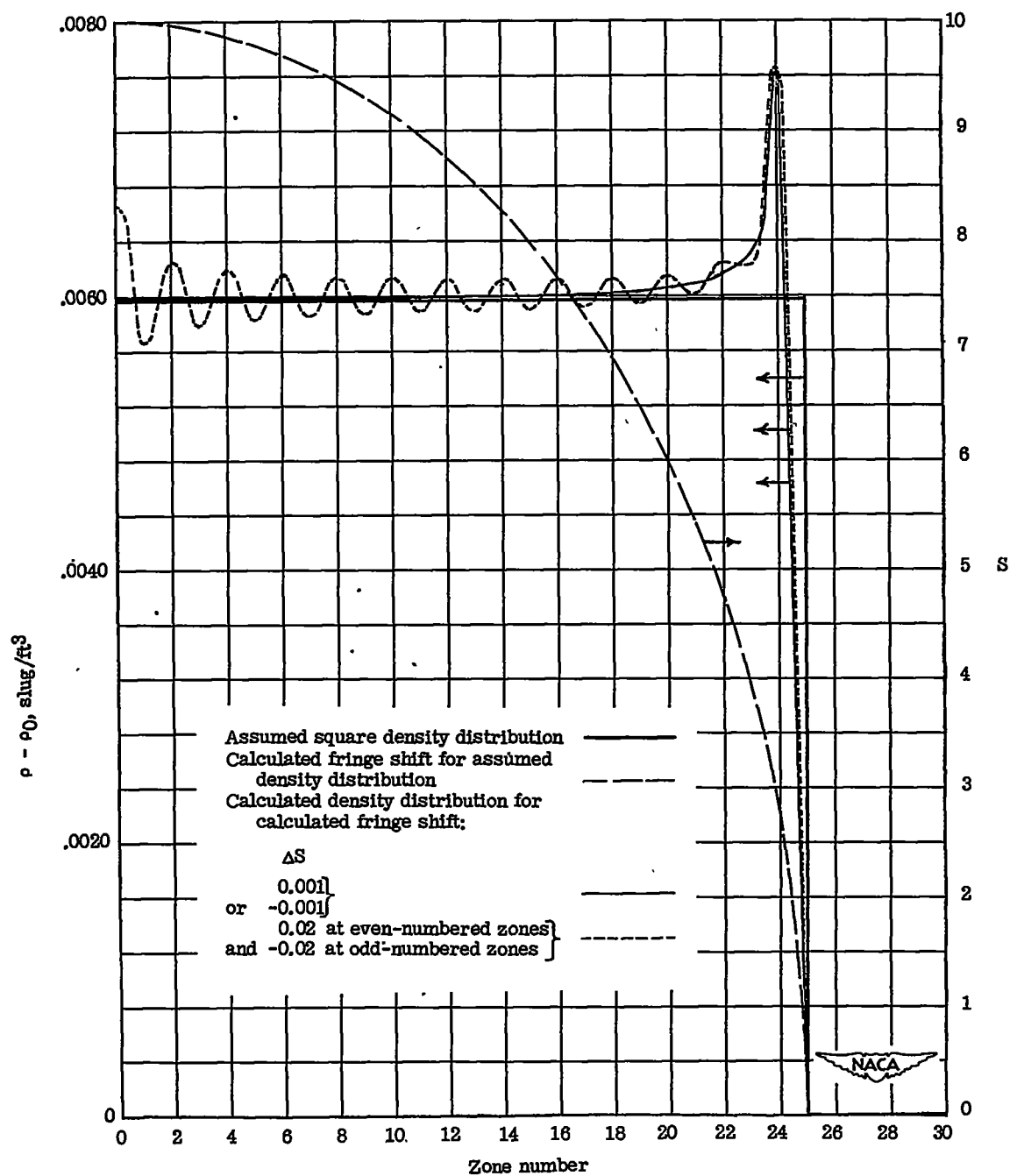


Figure 12.- Assumed distribution of density, corresponding distribution of fringe shift, and calculated distributions of density.

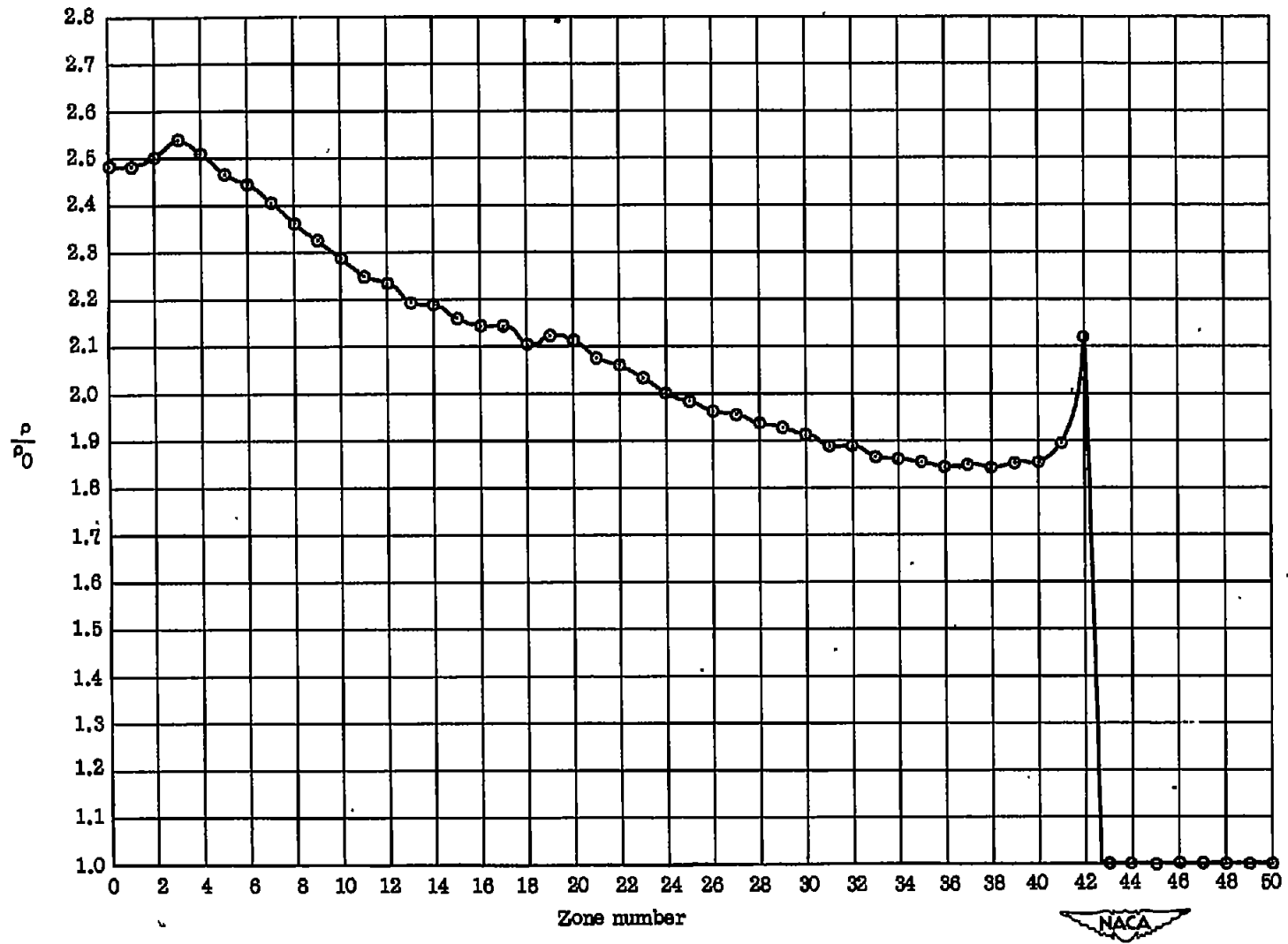


Figure 13.- Variation of ratio ρ/ρ_0 along typical cross section.